

AN *IN VIVO* INTERMEDIATE FILAMENT ASSEMBLY MODEL

STÉPHANIE PORTET AND JULIEN ARINO

Department of Mathematics
University of Manitoba, Winnipeg, MB, Canada

(Communicated by James Glazier)

ABSTRACT. A model is developed to study the *in vivo* intermediate filament organization in terms of repartition between four different structural states: soluble proteins, particles, short, and long filaments. An analysis is conducted, showing that the system has a unique, globally asymptotically stable equilibrium. By means of sensitivity analysis, the influence of parameters on the system is studied. It is shown that, in agreement with biological observations, posttranslational modifications of intermediate filament proteins resulting in filament solubilization are the main regulators of the intermediate filament organization. A high signalling-dependent solubilization of filaments favours the intermediate filament aggregation in particles.

1. Introduction. The cytoskeleton is a complex arrangement of structural proteins organized in three different networks: microfilaments, intermediate filaments, and microtubules. Each network has specific physical properties and spatial organization, and plays particular roles in the cell. Here, the focus is on the intermediate filament network, which is involved in the stabilization and mechanical resilience of the cell, cell migration, and signal transduction [6, 8].

Intermediate filaments are cell-type and differentiation-stage dependent. They are classified in five different types: Types I-IV are cytoplasmic filaments; Type V, lamins, are nuclear filaments. Intermediate filament proteins share a central rod domain that forms a highly conserved α -helix involved in the formation of coiled-coil structures [11]. The central rod domain is flanked by the head and tail domains, which are less conserved and confer specific structural properties to the different types of intermediate filament proteins. Mutations occur at the conserved central rod domain, which modulates the assembly; they then lead to defects in the organization of intermediate filament networks [1]. The head and tail domains contain the sites that can undergo posttranslational modifications [16, 18]; therefore, the terminal domains have mainly regulatory roles. The α -helical coiled-coil structures, called dimers, laterally associate to form tetramers. The latter are considered as the soluble subunits of intermediate filaments. Depending on the type of intermediate filament proteins, dimers are hetero- or homopolymers.

The *in vitro* assembly process of cytoplasmic intermediate filaments is initiated by a rapid lateral aggregation of tetramers into unit-length filaments (ULFs) [10];

2000 *Mathematics Subject Classification.* Primary: 92C37.

Key words and phrases. cytoskeleton assembly dynamics, intermediate filaments.

Research supported in part by NSERC.

this aggregation is directly followed by filament elongation, resulting from end-to-end annealing of ULFs and filaments [10, 13]. Evidence seems to indicate that tetramer addition to the filament ends does not contribute significantly to filament elongation [13]. Finally, the assembly process is terminated by a compaction event inducing a reduction of the filament diameter [10].

The *in vivo* assembly process of intermediate filament networks (Types I-IV) is also a multistage process: soluble proteins aggregate rapidly to constitute particles [5]. The ultrastructural organization of the particles is still not known; however, it is likely that they consist of filament precursors such as ULF [8], otherwise the emergence of the objects in the next stage of assembly, “squiggles” alias short filaments, that are longer than the restrictions imposed by the diffraction limit of the light microscope, would make no sense (in particular in the light of the *in vitro* data as published by Kirmse *et al.* [13]). These particles then grow and elongate into short filaments; particles are the precursors of filaments [21, 27]. Short filaments assemble into longer filaments which are also able to self-interact to create networks [5, 29]. Filaments are regulated by posttranslational modifications of intermediate filament proteins resulting in solubilizations and reorganizations [18, 22, 25].

The organization of a cytoskeletal network is the main determinant of its function in cells. Defects in the intermediate filament network organization are correlated to different human pathologies, such as skin fragility disorders, myopathies, and neurodegenerations [3, 15, 17]. Understanding mechanisms determining the intermediate filament network organization in cells, hence its cytopathological features in diseases, could lead to new therapies.

To the best of our knowledge, so far only a few mathematical models studying the organization of the intermediate filaments were developed. Beil *et al.* [2] investigate, with a nondynamical approach, the structural organization of cyokeratin networks by fitting stochastic tessellations to graph structures obtained by image segmentation of networks visualized by scanning electron microscopy. Brown *et al.* [4] use stochastic simulations to study the pulsatile motion of neurofilaments in axons. They do not describe the kinetics of neurofilament assembly. Craciun *et al.* [7] develop a deterministic analogue of the model in [4] and obtain comparable results in agreement with experimental data. Portet *et al.* [19] focus on the cyokeratin network organization in a cell in response to its extracellular mechanical environment. A hybrid model governing the soluble pool diffusion and the dynamics of individual filaments is introduced and simulations are conducted. In Portet *et al.* [20], two dynamical models of the *in vitro* and *in vivo* intermediate filament assembly are proposed, but the mathematical analysis is limited and no sensitivity analysis is conducted. In Kirmse *et al.* [13], the *in vitro* model in [20] is extended and its responses are compared to experimental data to determine the elongation mechanism of a vimentin filament.

The aim of the present work, which extends that of [20] in the *in vivo* case, is to model the assembly dynamics of *in vivo* intermediate filaments,

- to better understand the steps leading to the organization of the intermediate filament material,
- and to identify the major reactions acting on the whole process.

Here, the organization of the network is described in terms of the repartition of intermediate filament material between the different structural states that this material can be in: soluble proteins, particles, and short and long filaments.

2. Modelling concepts. It is assumed that the simplest intermediate filament structural state is the tetramer, which constitutes the pool of **soluble proteins** of intermediate filaments. Three other structural states for the intermediate filament material are considered: **particles**, **short filaments**, and **long filaments** [9]. The dynamics of these four structural states are governed by five reactions: particle formation, particle growth, filament formation, integration, and solubilization.

A particle is arranged from the soluble protein pool, **particle formation** is the aggregation of several soluble proteins to form particles [5]. The size of a particle is unknown [8]; a particle can take the form of an octamer (2 tetramers), ULF (8 tetramers), or a bigger structure. The size of a particle is defined here as the number of soluble proteins initially constituting a particle.

Particles grow by addition of soluble proteins [28]; this process is called the **growth of particles**. As lateral interactions between intermediate filament proteins can occur in three different manners [24], particle formation and growth of particles are described with different rates. Here, the particle is assumed to be the sole structural state recruiting from the soluble protein pool.

Particles convert to short filaments, this conversion is called **filament formation**. Particles are the precursors of filaments [21, 27]. Particles are considered here as nonfilamentous units in the sense that they are not yet components of the filamentous pool and cannot directly interact with filamentous units. Note, however, that the specific shape of objects such as the form of particles or the configuration of the networks are neither described nor addressed by the model.

Short filaments assemble to form longer filaments; short and long filaments also interact. These two mechanisms are described by the same rate; this hypothesis is supported by the fact that there exists a single mode of longitudinal interaction between intermediate filament proteins [24]. Based on observations made during *in vitro* assembly [13], it is also assumed that filament elongation results only from the interaction of filamentous units; soluble protein addition is considered as playing a significant role only in particle formation and growth. Filaments elongate and self-interact to form the network [28]. This set of processes (filament elongation and linking) is called **integration**. Intermediate filament linking does not require any associated proteins, and the integration of filaments to the network results solely from the interactions between long filaments. Consequently, for the sake of simplicity and because the model is expressed in mass, filament linking is not explicitly described in the integration. Here, long filaments are implicitly considered to constitute the networks.

Particles and short and long filaments can disassemble into soluble proteins; this is called **solubilization**. The solubilization of particles can result from the instability of the particle structure. The solubilization of filaments results from post-translational modifications of intermediate filament proteins in response to stress, apoptosis or mitosis (e.g., phosphorylation) [14, 18, 22, 23, 25]. Such signalling events can also cause particle solubilization.

Particle formation, particle growth, and integration of filaments are assumed to be biochemical events. Therefore, they are modelled using the Law of Mass Action. On the other hand, the conversion of particles into short filaments (the formation of filaments) is modelled as a structural event, a change of state, because little is known about the process involved. The initial number of soluble proteins involved in the formation of particles can also be interpreted as a structural feature.

TABLE 1. Parameters in the model.

Parameter	Signification
a	Initial number of soluble proteins in a particle
α	Rate of particle formation
π	Rate of growth of particles
ε	Rate of formation of a short filament
μ	Rate of assembly of two filaments
$\kappa_P(\cdot)$	Rate of solubilization of particles
$\kappa_F(\cdot)$	Rate of solubilization of filaments

3. **The model.** The model describes the dynamics of the four structural states of the intermediate filament material: soluble protein, particle (precursor of filaments), short filament, and long filament. So, four state variables are defined:

- $S(t)$, density of soluble proteins at time t ,
- $P(t)$, density of particles at time t ,
- $F_S(t)$, density of short filaments at time t , and
- $F_L(t)$, density of long filaments at time t .

The **soluble pool** is the state variable S . The **insoluble pool** consists of particles, short and long filaments, $P + F_S + F_L$. The **filamentous pool** is composed of short and long filaments, $F_S + F_L$.

Based on the modelling concepts above, the following system is obtained:

$$\frac{dS}{dt} = \underbrace{-\alpha S^a}_{\text{Particle formation}} \quad \underbrace{-\pi SP}_{\text{Particle growth}} \quad \underbrace{+\kappa_P(\cdot)P + \kappa_F(\cdot)(F_S + F_L)}_{\text{Solubilization}} \quad (1a)$$

$$\frac{dP}{dt} = \underbrace{\alpha S^a}_{\text{Particle formation}} \quad \underbrace{+\pi SP}_{\text{Particle growth}} \quad \underbrace{-\varepsilon P}_{\text{Filament formation}} \quad \underbrace{-\kappa_P(\cdot)P}_{\text{Solubilization}} \quad (1b)$$

$$\frac{dF_S}{dt} = \underbrace{\varepsilon P}_{\text{Filament formation}} \quad \underbrace{-\mu F_S^2 - \mu F_S F_L}_{\text{Integration}} \quad \underbrace{-\kappa_F(\cdot)F_S}_{\text{Solubilization}} \quad (1c)$$

$$\frac{dF_L}{dt} = \underbrace{\mu F_S^2 + \mu F_S F_L}_{\text{Integration}} \quad \underbrace{-\kappa_F(\cdot)F_L}_{\text{Solubilization}} \quad (1d)$$

The constant a represents the initial number of soluble proteins involved in a particle; it is assumed that $a \geq 2$. The aggregation rate of soluble proteins to form a particle is α . The constant π is the growth rate of particles. The constant ε represents the filament formation rate. The parameter μ represents the rate of assembly of filaments. The functions $\kappa_P(\cdot)$ and $\kappa_F(\cdot)$ represent the rate of solubilization of the particles and the filamentous pool, respectively. The rates of solubilization can take the form of a constant rate, a time-dependent function, or a concentration-dependent function of signalling proteins. All numbers and rate constants are positive; they are listed in Table 1.

System (1) is considered with nonnegative initial conditions such that $M_0 := S(0) + P(0) + F_S(0) + F_L(0) > 0$; *i.e.*, there is initially a positive concentration of proteins.

4. **Mathematical analysis.** Since $S' + P' + F'_S + F'_L = 0$, it follows that, defining

$$\Omega = \{(S, P, F_S, F_L) : S + P + F_S + F_L = M_0\},$$

Ω is positively invariant under the flow of system (1), and thus (1) is well-posed, with bounded nonnegative solutions.

The following result is a corollary of Theorem A.3, Appendix A. The existence and uniqueness of S^* is obtained in Theorem A.1, Appendix A.

Theorem 4.1. *Suppose that $\kappa_P(\cdot) \equiv \kappa_P \in \mathbb{R}_+$ and $\kappa_F(\cdot) \equiv \kappa_F \in \mathbb{R}_+$. Then system (1) has with respect to Ω the unique globally asymptotically stable equilibrium point*

$$\bar{E} := (\bar{S}, \bar{P}, \bar{F}_S, \bar{F}_L) = \left(M_0 S^*, \frac{M_0 \kappa_F}{\varepsilon + \kappa_F} (1 - S^*), M_0 F_S^*, M_0 F_L^* \right),$$

with S^* the only solution of

$$\mathcal{P}(S) = -\alpha(\varepsilon + \kappa_F) M_0^{\alpha-1} S^\alpha + \kappa_F(\varepsilon + \kappa_P - \pi M_0 S)(1 - S) = 0$$

that satisfies $0 < S^* < \min\left(1, \frac{\varepsilon + \kappa_P}{\pi M_0}\right)$, F_S^* given by

$$F_S^* = \frac{\varepsilon \kappa_F (1 - S^* - F^*)}{M_0 \varepsilon \mu (1 - S^* - F^*) + \kappa_F^2}$$

and F_L^* given by

$$F_L^* = \frac{\mu M_0 \varepsilon^2 (1 - S^* - F^*)^2}{\kappa_F (\mu M_0 \varepsilon (1 - S^* - F^*) + \kappa_F^2)},$$

where the equilibrium proportion of the filamentous pool F^* is

$$F^* = \frac{\varepsilon(1 - S^*)}{\varepsilon + \kappa_F}.$$

Interpretation: When particle and filament solubilization can occur, then starting with any initial structural configuration of the intermediate filament material, the system reaches an equilibrium distribution in which all structural states are present. The equilibrium distribution depends on parameter values. The level of filamentous pool is directly determined by the rate of network solubilization due to signalling.

The following result can be proved using the same arguments as in Appendix A, but for $\kappa_P(\cdot) \equiv \kappa_P \in \mathbb{R}_+$ and $\kappa_F(\cdot) \equiv 0$.

Corollary 4.2. *Suppose that $\kappa_P(\cdot) \equiv \kappa_P \in \mathbb{R}_+$ and $\kappa_F(\cdot) \equiv 0$. Then system (1) has with respect to Ω the globally asymptotically stable equilibrium*

$$\bar{E} = (\bar{S}, \bar{P}, \bar{F}_S, \bar{F}_L) = (0, 0, 0, M_0).$$

Interpretation: When there is no solubilization of the filamentous pool (no signalling), then starting with any initial configuration of the intermediate filament material, the system reaches an equilibrium at which all intermediate filament material is integrated in the network.

5. Numerical results. System (1) has seven parameters. For most of these parameters, the values are difficult to estimate. The first estimates of *in vitro* lateral and longitudinal aggregation rates of intermediate filament proteins were published only recently [13]. *In vivo* studies have established only the time scales of the processes involved [27, 28].

As the variation of the parameters of system (1) considered with constant rates does not induce any change of stability but changes the value of the unique positive equilibrium, a sensitivity analysis allows us to overcome the limitations resulting from the uncertainty on parameter values and to better understand how parameters influence the intermediate filament organization. Numerical simulations are then run to investigate the response of system (1) considered with time-dependent rates.

5.1. Constant rates $\kappa_F(\cdot) \equiv \kappa_F$ and $\kappa_P(\cdot) \equiv \kappa_P$: sensitivity analysis and numerical simulations. Understanding the influence of each reaction on the organization is very important, but characterizing reactions that determine the structural distribution of intermediate filaments is essential.

For instance, the value of the rate of particle growth depends on the molecular affinities of soluble proteins. If a mutation occurs on an intermediate filament gene, the affinity of soluble proteins can be modified [1, 15]. Hence, the value of the rate π can increase or decrease relative to a typical value. Also, cell signalling (mitosis, apoptosis, or mechanical stimulation) regulates posttranslational modifications of intermediate filament proteins resulting in the solubilization of the filamentous pool [14]; this is described in the model by the rate κ_F .

Sensitivity analysis allows the characterization of any change in structural state concentrations induced by the variation of a given parameter. Hence, influences of each reaction on the different structural states, and as a consequence on the whole intermediate filament organization, can be quantified.

Mathematical procedures used for performing the sensitivity analysis are summarized in Appendix B. To obtain sensitivities of various structural states to parameters, a system of $4 \times (7 + 1)$ equations consisting of (13) and (14) is numerically integrated with respect to time. Here transient behaviours are not examined, just the effect of parameters on the equilibrium values. To allow comparisons, normalized sensitivity coefficients (15) are used. Results of sensitivity analysis are shown in Figure 1, some illustrations of the dependence of equilibrium proportions on parameters are depicted in Figure 2, and the main conclusions are discussed below.

The initial size of particles, a , does not really change the organization: it mainly acts positively on the soluble pool and negatively on the insoluble pool. Results are not shown in Figure 2, as an increase of a does not induce any fundamental modification of the repartition of the states as the other parameters do.

High lateral aggregation rates, α and π , favour the insoluble pool. These parameters, which can be interpreted as rates of lateral aggregation of soluble proteins [24], affect similarly each structural state. High rates of lateral aggregation can modify the organization of intermediate filaments from a soluble configuration to an arrangement in networks (Figs. 2(a)-2(b)).

A high rate of conversion of particles to short filaments, ε , favours solubility. Particles are the only recruiters of soluble proteins: the faster particles convert to short filaments in comparison to the growth of particles (π), the lower the soluble pool

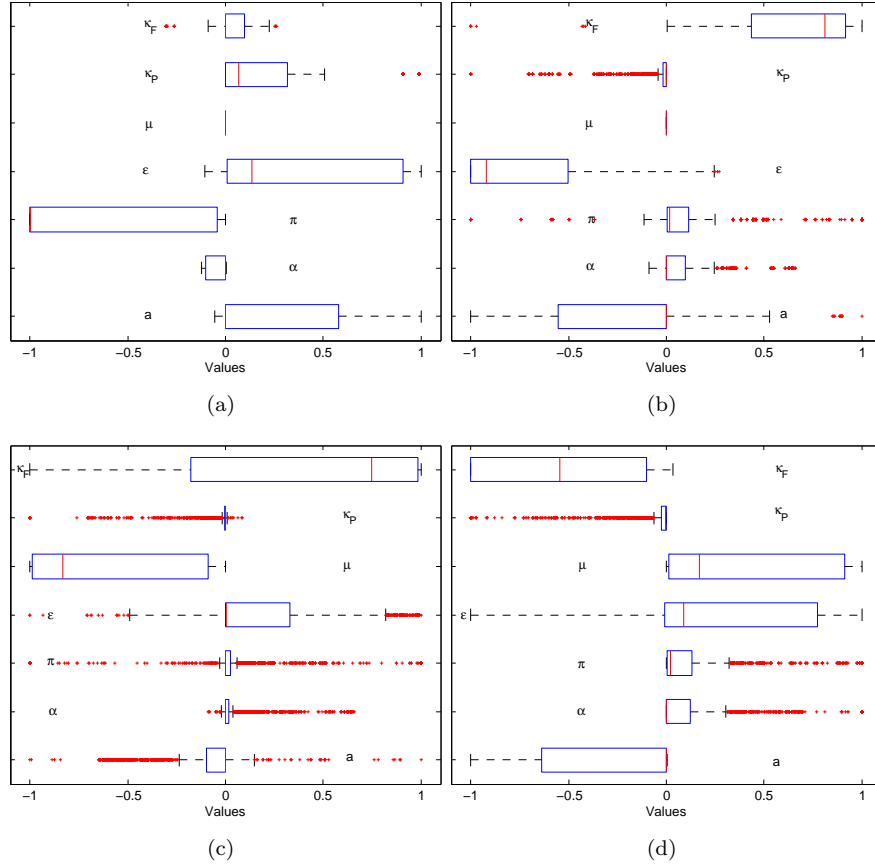


FIGURE 1. Normalized sensitivity coefficients of the structural states to the seven reactions estimated using (15): **(a)** soluble proteins, **(b)** particles, **(c)** filaments, and **(d)** filaments integrated in networks. For each structural state, computations were repeated for 4096 sets of parameters; results are displayed as boxplots for each parameter. The box shows the interquartile range. The median is indicated as the dividing line in the box. The length of the whiskers is specified as 1.5 times the interquartile range. All data with values beyond the ends of the whiskers are outliers, they are displayed with a + sign.

consumption. This explains the non-monotonic dependence of equilibrium proportions on ε (Figure 2(c)).

The rate of integration of filaments, μ , regulates the repartition of the filamentous pool. The proportion of filamentous pool stays constant, but the repartition of the filamentous pool between short and long filaments is modified. A high integration rate favours the organization of intermediate filament material in networks (Fig. 2(d)).

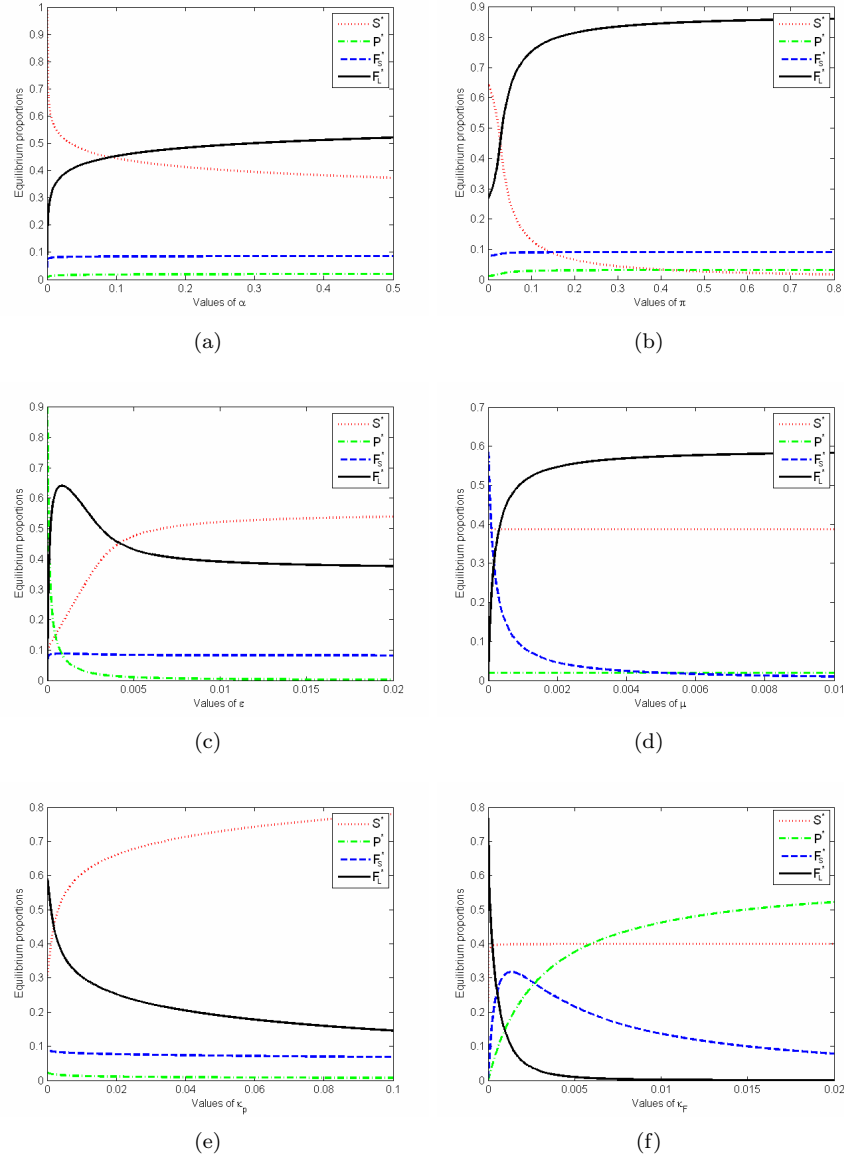


FIGURE 2. Influence of the rates α , π , ϵ , μ , κ_P and κ_F on equilibrium proportions.

The rate of solubilization of particles, κ_P , can affect the organization. An increase in κ_P can switch the repartition between the soluble and insoluble pool (Fig. 2(e)).

A high signalling-regulated filament solubilization rate, κ_F , favours particles. An increase in κ_F has opposite effects on filaments integrated in networks and particles, changing the organization of intermediate filaments from a network configuration to a particle configuration (Fig. 2(f)).

In biological terms, reactions related to the lateral assembly and disassembly of intermediate filament proteins (α , π , and κ_P), which can be affected by mutations [1], determine the structural organization of the intermediate filament material, and regulate the repartition between soluble and insoluble pools (mainly between soluble proteins and filaments integrated in networks). The signalling-regulated reaction (κ_F) totally determines the type of organization and favours particles [30].

5.2. Nonconstant rate $\kappa_F(t)$: numerical simulations. It is shown above that a main determinant of the intermediate filament organization is the rate of solubilization of filaments. Effects of non-constant rates of filament solubilization are now numerically investigated.

The rate $\kappa_F(\cdot)$ is taken to be a time-dependent function, with a baseline rate of solubilization and peaks resulting from signalling events. Two signalling events are considered here; they differ in duration and magnitude; they can be triggered by a mechanical stimulation or mitosis [14, 23].

The nonconstant rate of solubilization is defined as follows (bottom of Fig. 3)

$$\kappa_F(t) = \kappa_F + \kappa_m \exp^{-b(t-t_1)^2} + \kappa_M \exp^{-c(t-t_2)^2}, \quad (2)$$

with all parameters positive. Parameters t_1 and t_2 ($t_1 < t_2$) are times at which signalling events take place. Parameters b and c regulate the slope of the functions. Finally, κ_F represents the magnitude of the baseline solubilization rate of filaments, κ_m is the maximal magnitude of the rate of solubilization induced by the first signalling event, and κ_M is the maximal magnitude of the rate of solubilization resulting from the second signalling event ($\kappa_F \ll \kappa_m < \kappa_M$).

When the rate of filament solubilization κ_F is at its baseline level, intermediate filament material organizes in long filaments constituting networks. Interphasic cells have intermediate filaments organized in networks; the soluble pool represents a low proportion of the material, the major part is assembled in filaments [27].

Due to the first signalling event, the magnitude of κ_F starts increasing; consequently, the proportion of long filaments drops as they disassemble into soluble proteins that in turn aggregate in particles. Almost instantaneously, these particles convert into short filaments. The increase in the proportion of particles stops when the magnitude of the rate of filament solubilization decreases. For a while, short filaments are the dominant structural state. As the rate κ_F returns to its baseline level, the network reorganizes. This first signalling event can result from a mechanical stimulation that locally acts on the cell. The induced solubilization is not dramatic and induces the disassembly-reassembly of about 20% of the long filaments involved in the network; this can be interpreted as a local reorganization of the network in response to the stimulation.

The second signalling event induces a longer and stronger increase of the magnitude of the solubilization rate. Similarly as with the first signal, long filaments first disassemble, inducing an increase of the soluble pool followed by an increase of the proportion of particles and subsequently, an increase of the proportion of short filaments. For a while, particles dominate, and, as the magnitude of the solubilization rate decreases, short filaments reassemble and become the dominant structural state; finally the network reorganizes. In certain cell types, at metaphase, cells have a reduced filamentous pool, the intermediate filament material is mainly soluble or aggregated into granules and short rod shaped objects [27]. This second signal can therefore be interpreted as a mitosis, inducing an almost complete disassembly of the network of the cell before the reformation of networks in daughter cells.

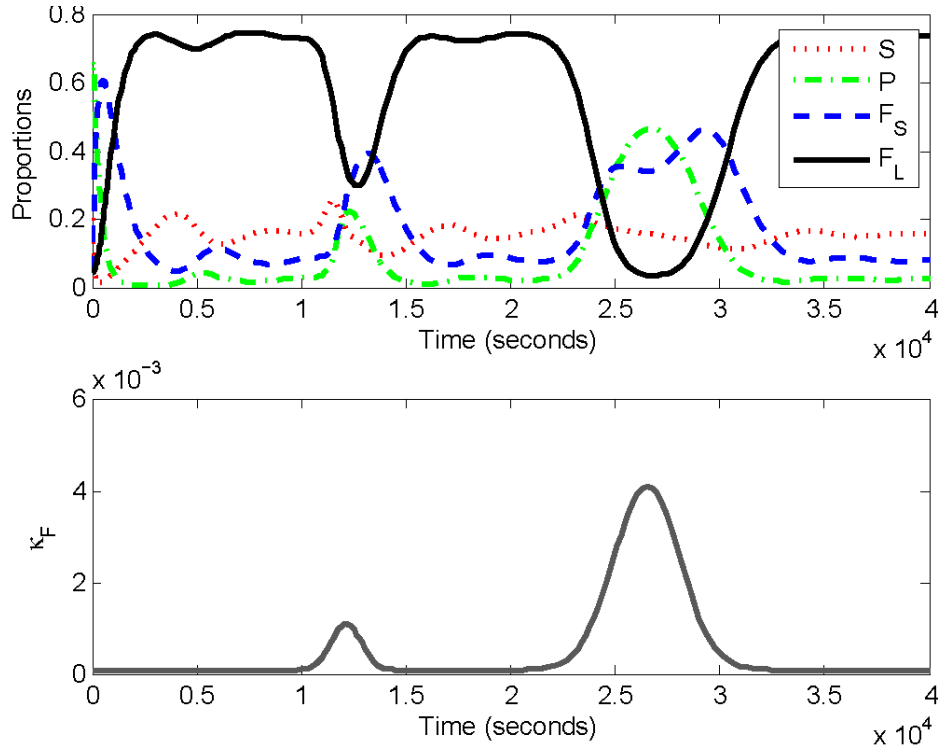


FIGURE 3. (Top) Temporal evolution (in seconds) of the proportions of intermediate filament material, with $a = 8$, $\alpha = 5 \times 10^{-3}$, $\pi = 2 \times 10^{-2}$, $\varepsilon = 3 \times 10^{-3}$, $\kappa_P = 10^{-4}$, $\mu = 10^{-3}$ and κ_F as in (2). (Bottom) Time-dependent rate of solubilization defined by (2). At about $t = 10000s$, a signal triggers posttranslational modifications of intermediate filament proteins resulting in an increase of the rate of solubilization with a maximal magnitude $\kappa_m = 10^{-3}$ at $t_1 = 12150s$. Similarly, at about $t = 22500s$, a second signalling event takes place, inducing a solubilization with a maximal magnitude $\kappa_m = 4 \times 10^{-3}$ at $t_2 = 26500s$. The baseline rate of solubilization is $\kappa_F = 10^{-4}$.

Note that similar results are obtained when using a square wave instead of a smooth function such as (2) for the non-constant rate of solubilization (results not shown).

6. Discussion. A nonlinear model for the dynamics of *in vivo* intermediate filaments is proposed; the model describes the assembly and the organization of this cytoskeletal component in terms of repartition between different structural states: soluble proteins, particles, short filaments, and filaments integrated in networks. The model includes several nonlinearities, one of which is of the form S^a . Because of these nonlinearities, the analysis is complicated. However, using mass conservation properties and the theory of asymptotically autonomous systems, it is shown that the system has a unique positive globally asymptotically stable equilibrium.

When signalling events occur ($\kappa_F \neq 0$), all structural states of intermediate filaments are present (Theorem 4.1). In the absence of signalling events ($\kappa_F = 0$), the intermediate filament material is entirely organized in networks (Corollary 4.2). In both cases, due to the global stability, there is no dependence on the initial configurations of the intermediate filament material. Moreover, the proportion of filamentous pool is inversely proportional to the rate of signalling-dependent solubilization of filaments κ_F . Qualitative behaviours of the model are in agreement with biological observations [27]: the organization of intermediate filament networks is mainly regulated by the filament solubilization [30], which can be interpreted as a consequence of posttranslational modifications.

By means of sensitivity analysis, reactions involved in intermediate filament assembly are studied to identify those that are the most determinant for the organization. The lateral aggregation of soluble proteins and the signalling-dependent solubilization of filaments are found to be the major regulators of this organization. The lateral aggregation of proteins acts on the solubility of the intermediate filament material. The signalling-dependent solubilization of filaments determines the intermediate filament organization and favours aggregation in particles. Furthermore, filament integration only modifies the distribution of the filamentous pool in terms of short and long filaments. This induces changes in the mechanical properties of networks.

More and more diseases have been associated with mutations of intermediate filament genes [17]. These mutations are not well understood, but they are known to affect the assembly of filaments and their integration in networks: the cytological signature of these diseases is a misorganization of the intermediate filament material. For example, in certain skeletal and cardiac myopathies, large aggregates of desmin are observed [1]. Furthermore, for several neurodegenerative diseases, intermediate filament aggregates also are a pathological hallmark; they seem to be correlated to high phosphorylations [23]. The putative effects of mutations on the network organization or the formation mechanisms of aggregates could be studied using models of the type proposed here.

Furthermore, the total length \mathbb{L} of intermediate filament material assembled into filaments can be computed from this model. Letting ℓ be the linear density of intermediate filaments [10], the total length \mathbb{L} can be expressed as

$$\mathbb{L}(t) = \frac{F_S(t) + F_L(t)}{\ell}.$$

The length \mathbb{L} is an experimentally observable quantity, which could help identify parameter values of the system, as this was done *in vitro* in [13].

The model has limitations; it does not specify the synthesis of the soluble pool, and motile properties of different structural states of intermediate filament material [9, 29] are not described. Depending on the cell type, antero and/or retrograde transports have been observed, with varying speeds for the different structural states of intermediate filaments. Some of those intracellular motions are related to the microtubule network, whereas others are microfilament network dependent [29]. Further work will extend the model by taking into account the motile properties of each structural state of the intermediate filament material.

Acknowledgements. The authors thank the editor and two anonymous referees, whose comments improved the present paper.

Appendix A. Proof of Theorem 4.1.

A.1. **Simplified models.** Summing the four equations in system (1), the conservation equation

$$\frac{d}{dt}(S + P + F_S + F_L) = 0$$

is obtained. Consequently, there holds that $S(t) + P(t) + F_S(t) + F_L(t) \equiv M_0$, that is, solutions are confined to the hyperplane $S + P + F_S + F_L = M_0$. Using $P(t) = M_0 - S(t) - F_S(t) - F_L(t)$, the dimensionality of system (1) can be reduced to 3. Considering the proportions $\bar{S} = S/M_0$, $\bar{F}_S = F_S/M_0$ and $\bar{F}_L = F_L/M_0$ of soluble pool, short filaments and long filaments in the cell, respectively, system (1) is now expressed as follows (bars are omitted)

$$\frac{dS}{dt} = -\alpha M_0^{a-1} S^a + (\kappa_P - \pi M_0 S)(1 - S - F) + \kappa_F F \quad (3a)$$

$$\frac{dF_S}{dt} = \varepsilon(1 - S - F) - \mu M_0 F_S^2 - \mu M_0 F_S F_L - \kappa_F F_S \quad (3b)$$

$$\frac{dF_L}{dt} = \mu M_0 F_S^2 + \mu M_0 F_S F_L - \kappa_F F_L, \quad (3c)$$

where $F := F_S + F_L$ is the filamentous pool. The dynamics of P (in proportions) is reconstructed from the state of system (3) using the fact that $P(t) = 1 - S(t) - F(t)$. This system is called the 3-dimensional system in proportions. Note that since for system (1), $S + P + F_S + F_L \equiv M_0$, the dynamics of (1) can be entirely reconstructed from the dynamics of (3) by multiplying variables of (3), as well as $P = 1 - S - F$, by M_0 . The two systems are therefore equivalent.

The dynamics of the filamentous pool F is obtained by summing equations (3b) and (3c), giving

$$\frac{dF}{dt} = \varepsilon(1 - S - F) - \kappa_F F.$$

Consequently, system (3) can be reduced to

$$\frac{dS}{dt} = -\alpha M_0^{a-1} S^a + (\kappa_P - \pi M_0 S)(1 - S - F) + \kappa_F F \quad (4a)$$

$$\frac{dF}{dt} = \varepsilon(1 - S - F) - \kappa_F F \quad (4b)$$

and the dynamics of P is deduced from $P(t) = 1 - S(t) - F(t)$. Model (4) is considered with nonnegative initial conditions $S(0) = s_0$, $F(0) = f_0$ and $P(0) = p_0 = 1 - s_0 - f_0$, with $s_0 + p_0 + f_0 = 1$.

System (3) has nonnegative solutions bounded above by 1, summing to 1 if the dynamics of $P(t)$ is also considered. Since system (4) is obtained by linear combination of variables of (1), the problem (4) is also well-posed, with solutions bounded above by 1, summing to 1 if the dynamics of $P(t)$ is also considered.

A.2. **Existence and stability of equilibria for the two-dimensional system (4).** First, the existence stability of equilibria of system (4) is considered. Let

$$\tilde{\Omega} = \{(S, P, F_S, F_L) : S + P + F_S + F_L = 1\}.$$

Theorem A.1. *Suppose that $\kappa_P(\cdot) \equiv \kappa_P \in \mathbb{R}_+$ and $\kappa_F(\cdot) \equiv \kappa_F \in \mathbb{R}_+$. Then system (4) has with respect to $\tilde{\Omega}$ a unique globally asymptotically stable equilibrium*

$$E^* = (S^*, F^*) := \left(S^*, \frac{\varepsilon(1 - S^*)}{\varepsilon + \kappa_F} \right),$$

where S^* is the only solution of

$$\mathcal{P}(S) = -\alpha(\varepsilon + \kappa_F)M_0^{a-1}S^a + \kappa_F(\varepsilon + \kappa_P - \pi M_0 S)(1 - S) = 0$$

that satisfies $0 < S^* < \min\left(1, \frac{\varepsilon + \kappa_P}{\pi M_0}\right)$.

Proof. Existence and uniqueness of the equilibrium E^ .*

To find the equilibria of system (4), consider its nullclines; an equilibrium point (S^*, F^*) is solution to the following system,

$$0 = -\alpha M_0^{a-1}S^a + (\kappa_P - \pi M_0 S)(1 - S - F) + \kappa_F F \quad (5a)$$

$$0 = \varepsilon(1 - S) - (\kappa_F + \varepsilon)F. \quad (5b)$$

From equation (5b), it is obtained that

$$F = \frac{\varepsilon(1 - S)}{\varepsilon + \kappa_F}. \quad (6)$$

Substituting (6) in (5a) implies that

$$0 = -\alpha(\varepsilon + \kappa_F)M_0^{a-1}S^a + \kappa_F(\varepsilon + \kappa_P - \pi M_0 S)(1 - S). \quad (7)$$

Thus, the positive roots S^* of (7) are the S components of the equilibrium solutions of (5). Rewriting (7) as

$$\mathcal{P}(S) = \Phi(S) - \Psi(S), \quad (8)$$

with

$$\Phi(S) = \kappa_F(\varepsilon + \kappa_P - \pi M_0 S)(1 - S)$$

and

$$\Psi(S) = \alpha(\varepsilon + \kappa_F)M_0^{a-1}S^a,$$

implies that the roots S^* lie at the intersections in \mathbb{R}_+^2 of Φ and Ψ .

The polynomial Ψ is an increasing function on \mathbb{R}_+ such that $\Psi(0) = 0$. Φ is a concave up parabola such that $\Phi(0) = \kappa_F(\varepsilon + \kappa_P) > 0$ and with 2 positive roots, 1 and $\frac{\varepsilon + \kappa_P}{\pi M_0}$. Φ decreases on $\left(0, \frac{\pi M_0 + \varepsilon + \kappa_P}{2\pi M_0}\right)$, increases on $\left(\frac{\pi M_0 + \varepsilon + \kappa_P}{2\pi M_0}, \infty\right)$, is positive on $\left(0, \min\left(1, \frac{\varepsilon + \kappa_P}{\pi M_0}\right)\right)$ and $\left(\max\left(1, \frac{\varepsilon + \kappa_P}{\pi M_0}\right), \infty\right)$. It follows that Ψ and Φ have a unique intersection for $0 < S < \min\left(1, \frac{\varepsilon + \kappa_P}{\pi M_0}\right)$. The second positive intersection, if it exists, has $S > \max\left(1, \frac{\varepsilon + \kappa_P}{\pi M_0}\right) \geq 1$.

Since state variables in system (4) are in proportions, a biologically relevant equilibrium must satisfy the condition $S \leq 1$. As a consequence, S^* is unique and satisfies

$$0 < S^* < \min\left(1, \frac{\varepsilon + \kappa_P}{\pi M_0}\right),$$

and system (4) has a unique interior equilibrium

$$E^* = \left(S^*, \frac{\varepsilon(1 - S^*)}{\varepsilon + \kappa_F}\right).$$

Stability of E^ .*

The Jacobian of system (4) at E^* is

$$J_{E^*} = \begin{pmatrix} -a\alpha M_0^{a-1} S^{*a-1} - \frac{\pi\kappa_F M_0}{\kappa_F + \varepsilon} (1 - S^*) & \pi M_0 S^* - \kappa_P + \kappa_F \\ +\pi M_0 S^* - \kappa_P & \\ -\varepsilon & -(\kappa_F + \varepsilon) \end{pmatrix}.$$

The trace of J_{E^*} is

$$\begin{aligned} \text{tr}(J_{E^*}) = & -a\alpha M_0^{a-1} S^{*a-1} + \frac{\pi M_0 (2\kappa_F + \varepsilon)}{\kappa_F + \varepsilon} S^* \\ & - \frac{\pi\kappa_F M_0 + (\kappa_P + \kappa_F + \varepsilon)(\kappa_F + \varepsilon)}{\kappa_F + \varepsilon}. \end{aligned} \quad (9)$$

Begin with the conclusion. In those regions in parameter space where the Jacobian matrix J_{E^*} has a negative trace, it follows from Bendixson's criterion that there are no nonconstant periodic solutions in the positive quadrant. It already has been shown that solutions of (4) are bounded. As the equilibrium E^* is unique, it follows from the Poincaré-Bendixson theorem that all trajectories limit to the equilibrium E^* , i.e. that the equilibrium E^* is globally asymptotically stable with respect to $\tilde{\Omega}$.

So now the sign of the trace of J_{E^*} is studied. Rewrite $\text{tr}(J_{E^*})$ as the difference between two polynomials in S^* ,

$$\text{tr}(J_{E^*}) = P_1(S^*) - P_2(S^*),$$

where

$$P_1(S^*) = \frac{\pi M_0 (2\kappa_F + \varepsilon)}{\kappa_F + \varepsilon} S^* - \frac{\pi\kappa_F M_0 + (\kappa_P + \kappa_F + \varepsilon)(\kappa_F + \varepsilon)}{\kappa_F + \varepsilon},$$

and

$$P_2(S^*) = a\alpha M_0^{a-1} S^{*a-1}.$$

The sign of $\text{tr}(J_{E^*})$ then depends on the relative positions of the graphs of P_1 and P_2 . The following observations can be made.

First, P_1 is an increasing function whose graph is a straight line with negative y -intercept,

$$-\frac{\pi\kappa_F M_0 + (\kappa_P + \kappa_F + \varepsilon)(\kappa_F + \varepsilon)}{\kappa_F + \varepsilon},$$

and a positive S^* -intercept denoted S_{int} ,

$$S_{int} := \frac{\pi\kappa_F M_0 + (\kappa_P + \kappa_F + \varepsilon)(\kappa_F + \varepsilon)}{\pi M_0 (2\kappa_F + \varepsilon)}.$$

Therefore, P_1 is negative for all $S^* < S_{int}$. On the other hand, P_2 is an increasing function with $P_2(0) = 0$, so P_2 is positive for all $S^* > 0$.

It follows that

$$\forall S^* \in [0, S_{int}], \quad P_1(S^*) < P_2(S^*),$$

which implies that $\forall S^* \in [0, S_{int}]$, $\text{tr}(J_{E^*}) < 0$.

Clearly, if $S_{int} \geq 1$, since $S^* < 1$, it follows that $\text{tr}(J_{E^*}) < 0$, giving the global stability of S^* . The condition $S_{int} \geq 1$ is equivalent to $\kappa_P + \kappa_F + \varepsilon \geq \pi M_0$.

Now suppose that $S_{int} < 1$, that is, $\kappa_P + \kappa_F + \varepsilon < \pi M_0$. This implies that $\min(\frac{\kappa_P + \varepsilon}{\pi M_0}, 1) = \frac{\kappa_P + \varepsilon}{\pi M_0}$, and therefore the case under consideration is that where $S^* \in (0, \frac{\kappa_P + \varepsilon}{\pi M_0}]$.

The relative positions of S_{int} and $\frac{\kappa_P + \varepsilon}{\pi M_0}$ are not known *a priori*, but note that if $\frac{\kappa_P + \varepsilon}{\pi M_0} \leq S_{int}$, then $(0, \frac{\kappa_P + \varepsilon}{\pi M_0}] \subset [0, S_{int}]$ and thus for any S^* , $P_1(S^*) < P_2(S^*)$, and thus S^* is globally asymptotically stable.

At this point, the result that S^* is globally asymptotically stable has been shown everywhere except in the case where S^* is between S_{int} and $\frac{\kappa_P + \varepsilon}{\pi M_0}$, with $S_{int} < \frac{\kappa_P + \varepsilon}{\pi M_0}$, that is,

$$\frac{\pi \kappa_F M_0 + (\kappa_P + \kappa_F + \varepsilon)(\kappa_F + \varepsilon)}{\pi M_0(2\kappa_F + \varepsilon)} < \frac{\kappa_P + \varepsilon}{\pi M_0}.$$

But this inequality is equivalent to $\pi M_0 - \kappa_P + \kappa_F < 0$, that is, $\pi M_0 < \kappa_P - \kappa_F$. However, the current case corresponds to $\kappa_P + \kappa_F + \varepsilon < \pi M_0$. Using both inequalities, there must hold that $\kappa_F + \varepsilon < -\kappa_F$, a contradiction. Therefore the case $S_{int} < (\kappa_P + \varepsilon)/(\pi M_0)$ is irrelevant.

It follows that $\text{tr}(J_{E^*}) < 0$, implying that E^* is globally asymptotically stable. \square

A.3. Existence and stability of equilibria for the three-dimensional system (3). In the system (3) at equilibrium, the variables S , F , and P take their equilibrium values S^* and F^* obtained in Theorem A.1, and $P^* = 1 - S^* - F^*$, respectively.

Since S and F converge to S^* and F^* , respectively, it follows that (3) is an asymptotically autonomous system, with limiting system

$$\frac{dF_S}{dt} = \varepsilon(1 - S^* - F^*) - \mu M_0 F_S^2 - \mu M_0 F_S F_L - \kappa_F F_S \quad (10a)$$

$$\frac{dF_L}{dt} = \mu M_0 F_S^2 + \mu M_0 F_S F_L - \kappa_F F_L. \quad (10b)$$

In (10), the dynamics of S and F , which reduce to $S(t) \equiv S^*$ and $F(t) \equiv F^*$, are omitted. The following result holds.

Theorem A.2. *Suppose that $\kappa_P(\cdot) \equiv \kappa_P \in \mathbb{R}_+$ and $\kappa_F(\cdot) \equiv \kappa_F \in \mathbb{R}_+ \setminus \{0\}$. Then system (10) has with respect to $\tilde{\Omega}$ a unique globally asymptotically stable equilibrium (F_S^*, F_L^*) , with*

$$F_S^* = \frac{\varepsilon \kappa_F (1 - S^* - F^*)}{M_0 \varepsilon \mu (1 - S^* - F^*) + \kappa_F^2} \quad (11)$$

and

$$F_L^* = \frac{\mu M_0 \varepsilon^2 (1 - S^* - F^*)^2}{\kappa_F (\mu M_0 \varepsilon (1 - S^* - F^*) + \kappa_F^2)}. \quad (12)$$

Proof. The value of the equilibrium $(F_S, F_L) = (F_S^*, F_L^*)$ is readily established. Also, at an arbitrary point (F_S, F_L) , the Jacobian matrix takes the form

$$\begin{pmatrix} -(2F_S + F_L)M_0\mu - \kappa_F & -\mu M_0 F_S \\ \mu M_0(2F_S + F_L) & \mu M_0 F_S - \kappa_F \end{pmatrix}$$

and has eigenvalues $-\kappa_F$ and $-\kappa_F - \mu M_0(F_S + F_L)$, so that the equilibrium (F_S^*, F_L^*) is locally asymptotically stable. Furthermore, the Jacobian has trace $-(F_S + F_L)M_0\mu - 2\kappa_F < 0$, so that Bendixson's criterion applies, implying, since solutions are bounded, that the equilibrium (F_S^*, F_L^*) is globally asymptotically stable for the limit system (10). \square

At this point, the following has been done/shown:

1. System (1) has solutions on the affine hyperplane $S(0) + P(0) + F_S(0) + F_L(0) = M_0$.

2. Therefore, system (1) can be transformed into a lower dimensional system, involving S , F_S , and F_L , with $P = M_0 - (S + F_S + F_L)$. Going to proportions, this is formulated as the 3-dimensional system (3). Systems (1) and (3) are equivalent, and therefore (3) is considered.
3. System (4), in the variables (S, F) , is then deduced from (3) by considering the compounded variable $F = F_S + F_L$.
4. System (4) has a unique, globally asymptotically stable equilibrium point (S^*, F^*) (Theorem A.1).
5. System (3) is then considered as a system in which $S(t)$ and $F(t)$ are time dependent quantities (and not obtained as solutions of a differential equation). Thus, (3) is of the form $x' = f(t, x)$, with $f(t, x) \rightarrow g(x)$ as $t \rightarrow \infty$, where g has $S = S^*$ and $F = F^*$. In this new system, called the limiting system of “(3) seen as a non-autonomous system”, the equation for S is trivial, so only (10) is studied.
6. For (10), it is shown in Theorem A.2 that there is a unique globally asymptotically stable equilibrium point (F_S^*, F_L^*) .

So it remains to show that the behaviour of system (3) in proportions can indeed be derived from the information obtained on S , F_S and F_L . Note that the method that is used in the proof of Theorem A.1 to establish the existence of S^* involves F_S and F_L only has a sum, *i.e.*, as $F = F_S + F_L$. The method is thus unchanged when considering F_S and F_L rather than F , and the conclusion still holds that there can be only one equilibrium value of S^* such that $0 < S^* < \min\left(1, \frac{\varepsilon + \kappa_F}{\pi M_0}\right)$. It is then easy to check that the equilibrium obtained from (3b) and (3c) with $F_S + F_L$ substituted to F in (3b), is the same to the one obtained for (10),

$$F_S^* = \frac{\varepsilon \kappa_F (1 - S^*)}{\kappa_F (\varepsilon + \kappa_F) + M_0 \varepsilon \mu (1 - S^*)}$$

and

$$F_L^* = \frac{\mu M_0 \varepsilon^2 (1 - S^*)^2}{(\varepsilon + \kappa_F) (\kappa_F (\varepsilon + \kappa_F) + M_0 \varepsilon \mu (1 - S^*))},$$

which are the values given by (11) and (12) in which $\frac{\varepsilon(1 - S^*)}{\varepsilon + \kappa_F}$ is substituted to F^* . Thus (3) also has a unique equilibrium.

From the theory of asymptotically autonomous differential equations, using for example Theorem 4.2 and Corollary 4.3 in [26], since the limit system (10) has the unique equilibrium point (S^*, F_S^*, F_L^*) , it follows that every forward orbit of (3) converges to (S^*, F_S^*, F_L^*) . As a consequence, the following result holds.

Theorem A.3. *The 3-dimensional system in proportions (3) has with respect to $\tilde{\Omega}$ the globally asymptotically stable equilibrium point $(S, F_S, F_L) = (S^*, F_S^*, F_L^*)$, with S^* given as in Theorem A.1, F_S^* given by (11) and F_L^* given by (12).*

From this, the value of P^* can be deduced. Since $P(t) = 1 - S(t) - F(t)$, it follows that

$$P^* := \lim_{t \rightarrow \infty} P(t) = 1 - S^* - F^* = \frac{\kappa_F (1 - S^*)}{\varepsilon + \kappa_F}.$$

The equilibrium values of S , P , F_S and F_L in (1) are then deduced by multiplying all terms by M_0 . This equilibrium is globally asymptotically stable for system (1).

Appendix B. Sensitivity analysis. System (1) can be expressed as follows

$$\frac{dy}{dt} = f(t, y, p) \quad (13)$$

where f is the right-hand side vector of (1), y is the 4-vector of state variables (S, P, F_S, F_L), and p is the 7-vector of parameters ($a, \alpha, \kappa_F, \kappa_P, \mu, \pi, \varepsilon$). Sensitivity of structural states with respect to parameter p_i , $i \in \{1, \dots, 7\}$, is defined as the 7-vector $\frac{\partial y(t)}{\partial p_i}$ satisfying the forward sensitivity equations,

$$\frac{d}{dt} \frac{\partial y(t)}{\partial p_i} = \frac{\partial f}{\partial y} \frac{\partial y}{\partial p_i} + \frac{\partial f}{\partial p_i}, \quad (14)$$

obtained by differentiating the original system (1) with respect to p_i and inverting the differentiation operators. The sensitivities are the derivatives of the model responses with respect to parameters; they represent the rates of change of structural state concentrations with respect to an increase in a given parameter p_i . To allow comparisons, normalized sensitivity coefficients defined by

$$\frac{p_i}{y} \frac{\partial y}{\partial p_i} \quad (15)$$

are considered. See, e.g., [12] for details.

In Figure 1, the sensitivities are obtained as follows. All parameters p_i are made to vary, giving a lattice, \mathcal{L} , in the 7-dimensional parameter space. The normalized sensitivity coefficient (15) of each structural state to each parameter is computed at each point in \mathcal{L} , and the values obtained for these sensitivity coefficients are used to generate the box plot.

REFERENCES

- [1] H. Bar, S. Strelkov, G. Sjoberg, U. Aebi and H. Herrmann, *The biology of desmin filaments: How do mutations affect their structure, assembly, and organisation?* J. Struc. Biol., **148** (2004), 137–52.
- [2] M. Beil, S. Eckel, F. Fletcher, H. Schmidt, V. Schmidt and P. Walther, *Fitting of random tessellation models to keratin filament networks*, J. Theor. Biol., **241** (2006), 62–72.
- [3] G. Benitez-King, G. Ramirez-Rodriguez, L. Ortiz and I. Meza, *The neuronal cytoskeleton as a potential therapeutical target in neurodegenerative diseases and schizophrenia*, Curr. Drug Targets CNS Neurol. Disord., **3** (2004), 515–33.
- [4] A. Brown, L. Wang and P. Jung, *Stochastic simulation of neurofilament transport in axons: the “stop-and-go” hypothesis*, Mol. Biol. Cell., **16** (2005), 4243–55.
- [5] L. Chang, Y. Shav-Tal, T. Trcek, R. Singer and R. D. Goldman, *Assembling an intermediate filament network by dynamic cotranslation*, J. Cell Biol., **172** (2006), 747–58.
- [6] P. A. Coulombe and P. Wong, *Cytoplasmic intermediate filaments revealed as dynamic and multipurpose scaffolds*, Nature Cell Biol., **6** (2004), 699–706.
- [7] G. Craciun, A. Brown and A. Friedman, *A dynamical system model of neurofilament transport in axons*, J. Theor. Biol., **237** (2005), 316–22.
- [8] R. D. Goldman, B. Grin, M. G. Mendez and E. R. Kuczumarski, *Intermediate filaments: versatile building blocks of cell structure*, Cur. Opin. Cell Biol., **20** (2008), 28–34.
- [9] B. T. Helfand, L. Chang and R. D. Goldman, *Intermediate filaments are dynamic and motile elements of cellular architecture*, J. Cell Sci., **117** (2004), 133–41.
- [10] H. Herrmann, M. Haner, M. Brettel, N.-O. Ku and U. Aebi, *Characterization of distinct early assembly units of different intermediate filament proteins*, J. Mol. Biol., **286** (1999), 1403–20.
- [11] H. Herrmann and U. Aebi, *Intermediate filaments and their associates: multi-talented structural elements specifying cytoarchitecture and cytodynamics*, Curr. Op. Cell Biol., **12** (2000), 79–90.
- [12] B. Ingalls and H. M. Sauro, *Sensitivity analysis of stoichiometric networks: an extension of metabolic control analysis to non-steady state trajectories*, J. Theor. Biol., **222** (2003), 23–36.

- [13] R. Kirmse, S. Portet, R. Mücke, U. Aebi, H. Herrmann and J. Langowski, *A quantitative kinetic model for the in vitro assembly of intermediate filaments from tetrameric vimentin*, J. Biol. Chem., **282** (2007), 18563–72.
- [14] N.-O. Ku, S. Azhar and M. B. Omary, *Keratin 8 phosphorylation by p38 kinase regulates cellular keratin filament reorganization*, J. Biol. Chem., **227** (2002), 10775–82.
- [15] E. B. Lane and W. H. I. McLean, *Keratins and skin disorders*, J. Pathol., **204** (2004), 355–66.
- [16] M. B. Omary, N. Ku, J. Liao and D. Price, *Keratin modifications and solubility properties in epithelial cells and in vitro*, Subcell Biochem., **31** (1998), 105–40.
- [17] M. B. Omary, P. A. Coulombe and W. H. McLean, *Intermediate filament proteins and their associated diseases*, New Engl. J. Med., **351** (2004), 2087–100.
- [18] M. B. Omary, N.-O. Ku, G.-Z. Tao, D. M. Toivola and J. Liao, *“Heads and Tails” of intermediate filament phosphorylation: Multiple sites and functional insights*, Trends Biochem. Sci., **31** (2006), 383–94.
- [19] S. Portet, O. Arino, J. Vassy, and D. Schoevaert, *Organization of the cytokeratin network in an epithelial cell*, J. Theor. Biol., **223** (2003), 313–33.
- [20] S. Portet, J. Vassy, C. W. Hogue, J. Arino and O. Arino, *Intermediate filament networks: in vitro and in vivo assembly models*, CR: Biol., **327** (2004), 970–76.
- [21] V. Prahlad, M. Yoon, R. D. Moir, R. D. Vale and R. D. Goldman, *Rapid movements of vimentin on microtubule tracks: kinesin-dependent assembly of intermediate filament networks*, J. Cell Biol., **143** (1998), 159–70.
- [22] K. M. Ridge, L. Linz, F. W. Flitney, E. R. Kuczmarski, Y.-H. Chou, M. B. Omary, J. I. Sznajder and R. D. Goldman, *Keratin 8 phosphorylation by protein kinase C δ regulates shear stress-mediated disassembly of keratin intermediate filaments in alveolar epithelial cells*, J. Biol. Chem., **280** (2005), 30400–5.
- [23] R. K. Sihag, M. Inagaki, T. Yamaguchi, T. B. Shea and H. C. Pant, *Role of phosphorylation on the structural dynamics and function of type III and IV intermediate filaments*, Exp. Cell Res., **313** (2007), 2098–109.
- [24] P. Steinert, L. Marekov and D. Parry, *Diversity of intermediate filament structure: evidence that the alignment of coiled-coil molecules in vimentin is different from that in keratin intermediate filaments*, J. Biol. Chem., **268** (1993), 24916–25.
- [25] P. Strnad, R. Windoffer and R. E. Leube, *Induction of rapid and reversible cytokeratin filament network remodeling by inhibition of tyrosine phosphatases*, J. Cell Sci., **115** (2002), 4133–48.
- [26] H. R. Thieme, *Convergence results and a Poincaré-Bendixson trichotomy for asymptotically autonomous differential equation*, J. Math. Biol., **30** (1992), 755–63.
- [27] R. Windoffer and R. E. Leube, *De novo formation of cytokeratin filaments networks originates from the cell in A-431 cells*, Cell Motil. Cytoskeleton, **50** (2001), 33–44.
- [28] R. Windoffer, S. Woll, P. Strnad and R. E. Leube, *Identification of novel principles of keratin filament network turnover in living cells*, Mol. Biol. Cell, **15** (2004), 2436–48.
- [29] S. Woll, R. Windoffer and R. E. Leube, *Dissection of keratin dynamics: different contributions of the actin and microtubule systems*, Eur. J. Cell Biol., **84** (2005), 311–28.
- [30] S. Woll, R. Windoffer and R. E. Leube, *MAPK-dependent shaping of the keratin cytoskeleton in cultured cells*, J. Cell Biol., **177** (2007), 795–807.

Received December 11, 2007; Accepted September 1, 2008.

E-mail address: portets@cc.umanitoba.ca

E-mail address: arinoj@cc.umanitoba.ca